Injury to tissue caused by device penetration of the skin triggers formation of extracellular traps

Check for updates

Kenneth A. Wood[1], Priscila S. Cunegundes[1], Jean G. de Souza [1], Joseph Cavataio [1], Tejas Kakunje[1], Don L. Kreutzer[2] & Ulrike Klueh [1] ✉

Continuous glucose monitoring (CGM) systems are vital for diabetes management, but sensor performance is often compromised by host immune responses following insertion. This study investigates early tissue and immune reactions, focusing on neutrophil extracellular trap (NET) formation, or NETosis. In porcine models, insertion trauma rapidly induced NETosis, preceding vascular regression and fibrotic encapsulation—processes that may hinder glucose diffusion and impair sensor accuracy. In a murine air pouch model, sensor implantation elevated inflammatory cytokines (IL-6, KC/GRO) and neutrophil infiltration within 24 hours. Scanning electron microscopy revealed NETs exclusively in traumatized tissue. Notably, neutrophils from type 2 diabetes patients failed to undergo NETosis on polyurethane surfaces in vitro, suggesting impaired immune responses due to metabolic dysfunction. These findings identify NETosis as a key driver of early sensor-tissue interactions. Strategies to reduce insertion trauma and modulate NET formation may enhance CGM reliability and longevity, informing future improvements in sensor design and deployment.

Diabetes ranks as the fourth leading cause of death in the developing world, mainly due to its debilitating microvascular and macrovascular complications[1,2]. Over the past two decades, advancements in diabetes technology have revolutionized the care of individuals with diabetes[3]. Notably, continuous glucose monitoring (CGM) has improved management by increasing Time in Range, which indicates the duration of acceptable blood glucose levels, and by decreasing diabetic complications[4,5]. Although commercial transdermal glucose sensors now last over 10 days, this limited lifespan requires multiple implantations at different skin sites. A major challenge with sequential site implantation is the limited available skin area, especially in pediatric patients. Therefore, maintaining healthy tissue at CGM implantation sites is essential for repeated device placements. Diabetes devices can trigger tissue responses after implantation, including the formation of scar tissue, which can threaten tissue health and compromise future device implantation[6,7]. Identifying and addressing the underlying causes of immune reactions at the sensor-tissue interface is crucial for preserving tissue integrity.

Inflammation, especially the accumulation of leukocytes at the sensor-tissue interface, followed by fibrotic encapsulation, decreases the effectiveness of glucose monitoring devices[8,9]. A foreign body response driven by macrophages is considered an unavoidable outcome of prolonged device implantation, which promotes fibrosis[10–12]. This study aims to characterize the in vitro cytotoxicity, in vivo tissue toxicity, and pro-inflammatory activity of commercial glucose sensors, using Libre 2 as our standard model. By combining in vitro approaches with two animal models (murine and swine), we independently examine cellular and tissue responses to sensor coatings and assess the cumulative effects of device insertion and prolonged implantation. Commercial continuous glucose monitor (CGM) devices use an applicator to insert the sensor beneath the skin. These applicators often depend on spring-loaded needle inserters. They are not suitable for testing in mice because the length of the insertion needle exceeds the thickness of murine skin, piercing beyond the subcutaneous layer and risking injury to underlying tissues. In vitro toxicity studies were conducted to determine whether sensor coatings have a significant impact on inflammatory activity. Neutrophils were isolated from the blood of healthy donors and donors with diabetes. In mice, sensors were placed without penetrating trauma to isolate coating-specific tissue reactions.

Libre 2 sensors were inserted into non-diabetic Yucatan swine to assess the combined effects of sensor insertion, coating, and inflammatory response over a 3-week period. Swine are the preferred animal model in diabetes device research due to their skin structure, wound healing, and immune responses, which closely resemble those of humans[13,14]. These similarities encompass wound closure through re-epithelialization and the formation of granulation tissue, which aids tissue repair and regeneration.

[1]Wayne State University, Integrative Biosciences Center (IBio), Detroit, MI, USA. [2]University of Connecticut School of Medicine, Department of Surgery, Farmington, CT, USA. ✉e-mail: Menkes@wayne.edu

This makes them ideal for evaluating sensor biocompatibility and long-term performance. Miniature swine breeds, such as the Yucatan, offer practical advantages: they are easier to handle than domestic swine due to their smaller size, yet still large enough to accommodate devices designed for human use. These studies identified specific tissue responses caused by insertion trauma, material composition, and prolonged presence. The findings will support the development of next-generation CGM systems, including improved insertion techniques, to protect tissue health and enhance long-term diabetes management.

Results

Regression in neovascularization near the sensor is evident by 3 weeks

Using the non-diabetic porcine model, we assessed the tissue reactions triggered by the commercial glucose sensor. These glucose sensor devices are implanted into the subcutaneous skin tissue using a spring-actuated insertion mechanism. Figure 1A displays representative images of tissue biopsy sections stained with H&E, trichrome, and anti-CD31 at 1-, 7-, 14-, and 21-days post-insertion. On Day 1 following sensor insertion, acute inflammatory responses were mainly noted in the skin's subcutaneous adipose layer and the immediate proximity of the device. Higher image resolution reveals an abundance of neutrophils surrounded by deep, purple-stained threads resembling web-like neutrophil extracellular traps (NETs), manifesting neutrophil death. Only non-specific anti-CD31 staining is noted in the subcutaneous dermal layer at the sensor insertion site (Supplementary Fig. 1 showing high-resolution images).

On Day 7, inflammation extended into the dermis near the sensor. The subcutaneous fat exhibited granulomatous inflammation mainly involving macrophages and isolated multinucleated giant cells. The inflammatory process also included infiltration by neutrophils, occasional lymphocytes, eosinophils, and basophils. The strongest response in the subcutaneous tissue surrounded the granulation tissue, with evenly distributed new blood vessel formation. Wispy collagen fibers along the inflammatory track are also visible, as depicted in the trichrome stain. By Day 14, the subcutaneous skin exhibited increased fibrosis, fibrin deposition, inflammation, and fat necrosis compared to the decreasing vascularity near the sensor. This reduction in new blood vessels around the sensor becomes even more apparent on Day 21, when vessels are farther from the sensor. At Day 21, fibrosis dominates the tissue response, with neovascularization mostly restricted to the outer edge of the sensor—presumably to support local fibroblasts. To evaluate vascular changes over time, we used CD31 immunostaining to measure the distance between blood vessels and the glucose sensor–tissue interface. As shown in Fig. 1B, the average vessel distance increased from $59 \pm 24\ \mu m$ at Day 7 to $63 \pm 21\ \mu m$ at Day 14, reaching $106 \pm 25\ \mu m$ by Day 21 (Supplementary Fig. 2). This progressive increase indicates ongoing vascular regression. Similar trends have been reported in studies of subcutaneous implants and foreign body responses, where initial injury induces angiogenesis that later diminishes due to chronic inflammation, fibrotic encapsulation, or declining metabolic demand[11,15]. The marked increase in vessel distance by Day 21 suggests significant vessel loss during the late phase of tissue remodeling, which may impair nutrient diffusion and contribute to sensor signal degradation. These findings align with a chronic inflammatory response that shifts to dense fibrosis, a hallmark of wound healing, which ultimately leads to scar formation and may make the site less suitable for future sensor implantation.

Extracellular trap formation is dominant on day 1 following sensor insertion

We conducted a quantitative fluorescent staining analysis of the respective biopsy tissue sections to confirm the formation of NETs. Extracellular traps (ETs) are structures composed of decondensed DNA decorated with proteins from cytoplasmic granules[16]. Although ETs are beneficial in trapping and neutralizing pathogens, mainly when phagocytosis is unattainable, excessive or dysregulated ET formation can contribute to tissue damage and inflammation[17–21]. Neutrophils, macrophages, mast cells, and eosinophils

can induce ET formation, a process known as ETosis[16,22]. NETs were explicitly identified using sequential triple staining of DAPI, neutrophil elastase, and myeloperoxidase (MPO) on day 1. NETs dominated the tissue reaction and followed the sensor insertion path at 1-day post-sensor insertion (Fig. 2). For subsequent time points, ETs were identified in the sensor tissue biopsy using the non-specific DNA markers DAPI and citrullinated histone H3 (CitH3), including MPO. MPO is a heme-containing enzyme highly abundant in the azurophilic granules of neutrophils. While monocytes also produce MPO, their expression levels are significantly lower than those of neutrophils. Although ETs were sporadically observed over the entire 3-week implantation period, they were most evident following sensor insertion (Fig. 2). Macrophages may exhibit weak MPO staining in inflamed tissues, particularly following the phagocytosis of neutrophil debris. ET appearance was more substantial on day 7 post-sensor insertion than during the following 2 weeks. Overall, ETs decreased with the appearance of fibrosis over the 3 weeks following sensor implantation.

Acute inflammation primes the device surface for the formation of extracellular traps

In mice, the tissue response to the sensing material is assessed without causing additional tissue damage from spring-actuated insertion. The sensing material was placed into non-diabetic mice, both with and without an air pouch, to determine if the sensor coating triggers extracellular trap formation. The air pouch model involves creating a subcutaneous cavity by injecting air into the dorsal skin of the mouse. Subsequently, immune cells infiltrate the space, and inflammatory mediators are released in response to the inserted sensing material, which can then be studied[23,24]. Glucose sensors inserted into mice without an air pouch showed minimal cellular attachment and no extracellular DNA staining, as confirmed by SEM (Fig. 3A).

In contrast, sensors removed from the air pouch manifested significant cellular attachment and extensive extracellular DNA (Fig. 3A). As sensor removal from mouse tissue was performed using the same procedure regardless of the presence or absence of an air pouch, this suggests that acute inflammation is required to prime the device surface for extracellular trap formation. Thus, the air pouch initiates an acute inflammatory response independent of the sensor material.

Lavage of the mouse air pouch also provided additional insights into leukocyte influx and the expression of pro-inflammatory cytokines. Cellular leukocyte subtype analysis following 1- and 3-day post-sensor insertion into the air pouch demonstrated significantly higher neutrophil counts at 1-day post-sensor insertion than in the sham group (Fig. 3D). There was no significant difference in the monocyte, macrophage, mast cell, and lymphocyte populations among the treatment groups for both days assessed (Fig. 3B, C, E, F).
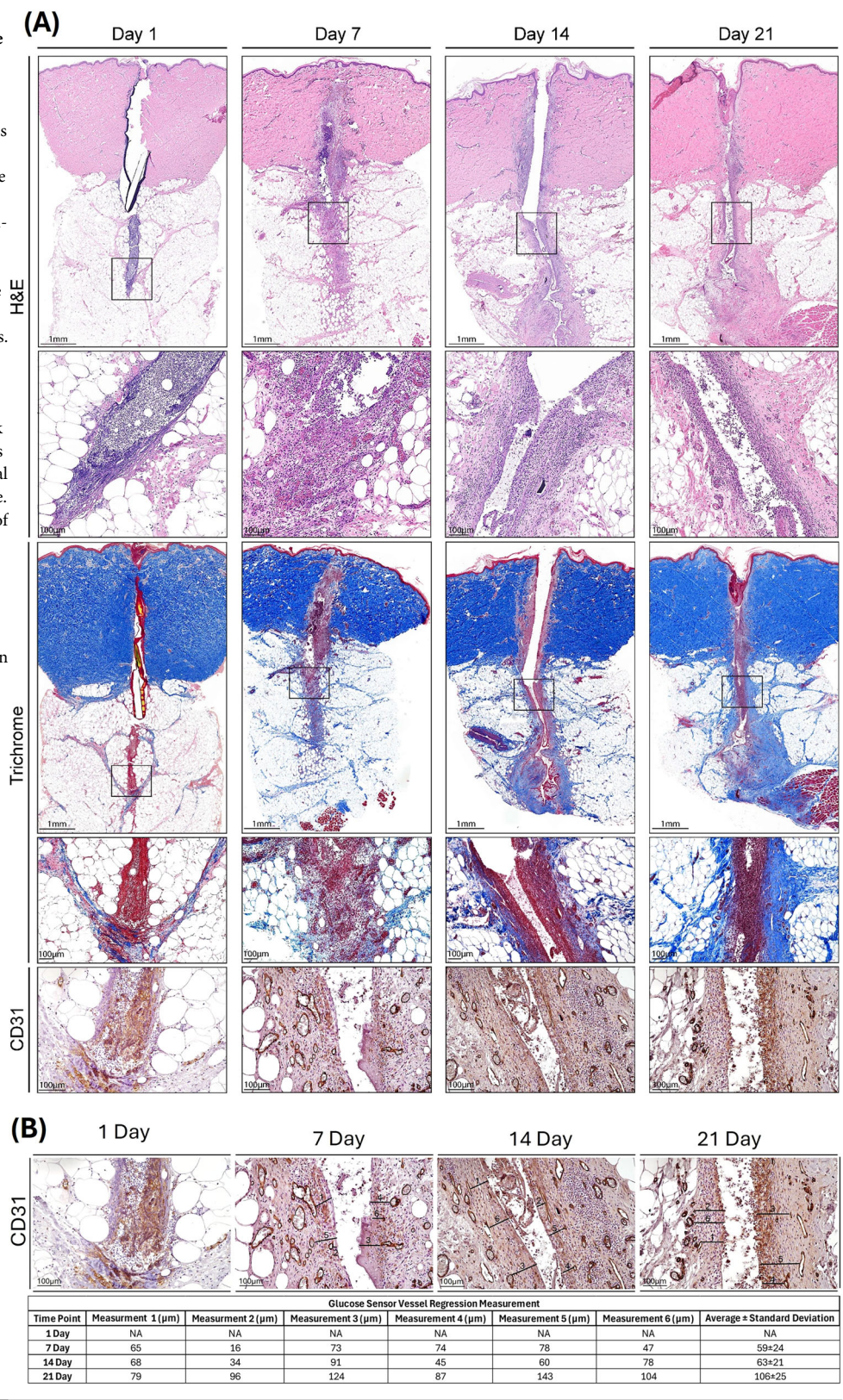
These studies demonstrated that the sensor device induced a significant expression of the pro-inflammatory cytokine IL-6 on both day 1 and day 3 (Fig. 3J). Concurrently, the chemokine KC/GRO reached significantly higher concentrations only on the first day following sensor insertion (Fig. 3K). Histopathologic comparison of the air pouch tissue from the sham group and the sensor-adjacent tissue revealed the same minimal tissue reactions lining the air pouch interface on both days evaluated (Fig. 3L). This further confirms that the sensor material does not substantially contribute to the tissue reaction in the early days following sensor insertion.

Neutrophils isolated from the blood of T2D patients do not exhibit NET formation on the polyurethane coating

On day 1 after sensor insertion, a higher neutrophil count (Fig. 3A), including NET formation, dominated the tissue response (Fig. 2). Thus, we utilized neutrophils isolated from a diabetic patient population to further investigate cell-material interactions. It is known that diabetes primes neutrophils to undergo NET formation, a process known as NETosis[25]. Thus, we hypothesized that any surface exposed to neutrophils isolated from the blood of diabetic donors would exhibit increased NETosis. To test this
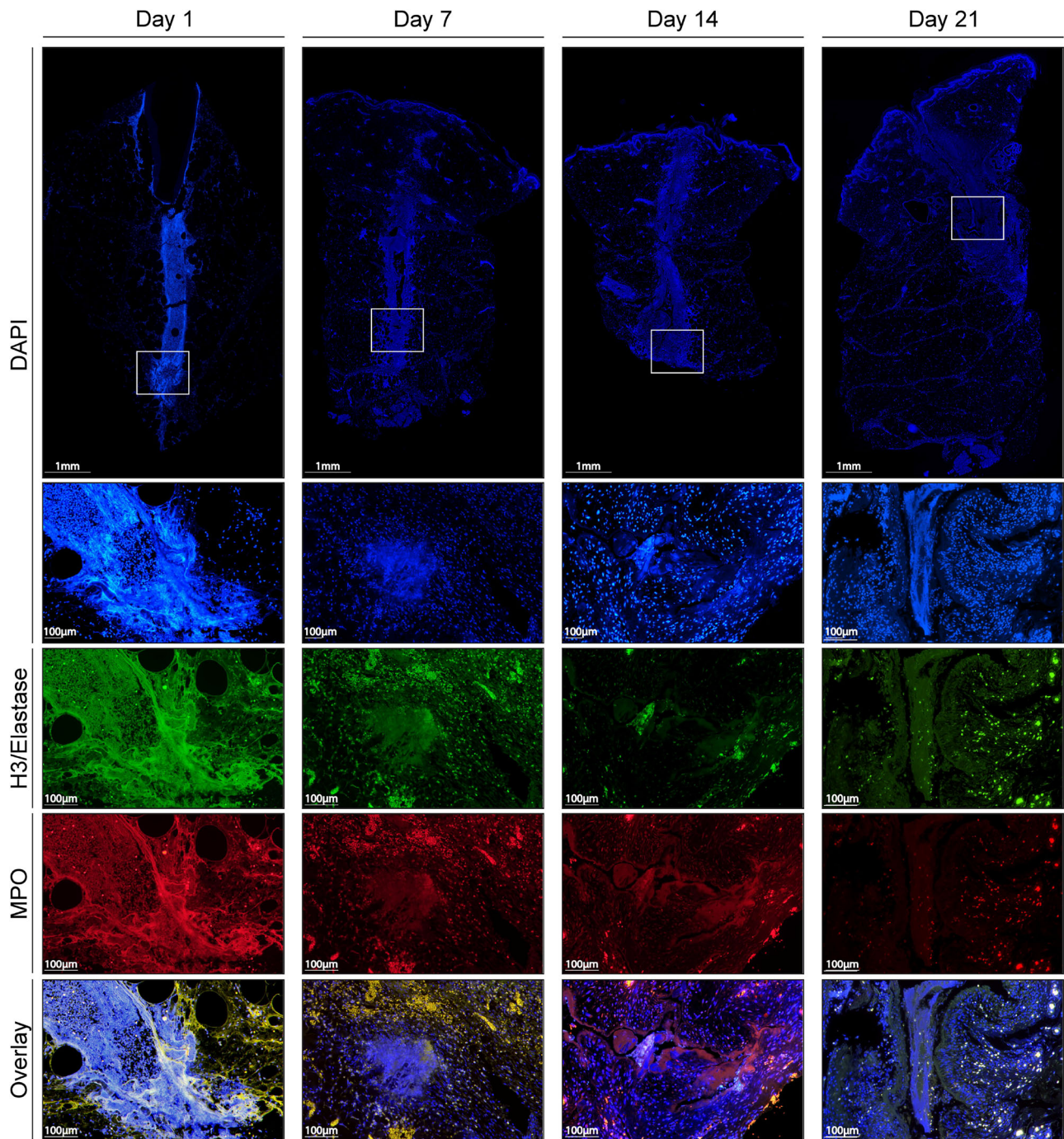
Fig. 1 | Histopathological evaluation of tissue reactions in swine induced by implanted glucose sensor devices. A To assess tissue reactions at the sensor implantation site, tissue samples were obtained through biopsy at 1 day, 7-, 14- and 21-days post-device insertion. The resulting tissue was processed for histopathologic evaluation using Hematoxylin and Eosin (H&E) staining, trichrome staining, and immunostaining for vascularization (CD31). H&E and trichrome stains depict magnification (1×), representing a 1 mm scale bar. Black rectangles represent higher magnification (20×) with scale bars indicating 100 μm. H&E shows the nuclear staining of inflammatory infiltrates, while the trichrome stain shows the production of fibrosis. Vessel regression was observed as early as 2 weeks post-sensor implantation, as indicated by the CD31 stain. Particularly at 3 weeks, all vessels are located in the periphery of the device's tissue track and at the edge of fibrosis. **B** Vessel regression was assessed by measuring the distance from individual blood vessels to the glucose sensor–tissue interface. At each time point, six vessels (three on each side of the sensor) were measured using ImageJ, and the measurements were calibrated to a 100 μm spatial scale. The average vessel distance increased over time, indicating progressive vascular regression. Averages are reported ± the standard deviation. Corresponding high-resolution images are shown in Supplementary Fig. 1.

Glucose Sensor Vessel Regression Measurement						
Time Point	Measurement 1 (μm)	Measurement 2 (μm)	Measurement 3 (μm)	Measurement 4 (μm)	Measurement 5 (μm)	Measurement 6 (μm)	Average ± Standard Deviation
1 Day	NA	NA	NA	NA	NA	NA	NA
7 Day	65	16	73	74	78	47	59±24
14 Day	68	34	91	45	60	78	63±21
21 Day	79	96	124	87	143	104	106±25

hypothesis, neutrophils were isolated from the blood of individuals with and without type 2 diabetes (T2D) using two different neutrophil isolation methods. Levels of NETs on the polyurethane-coated and uncoated surfaces were then measured and compared. Two isolation methods were utilized, as it is now understood that any method other than the immunomagnetic method stimulates neutrophils toward NETosis[26]. When neutrophils derived from healthy volunteer blood or T2D blood were exposed to either the polyurethane-coated or uncoated surfaces, only neutrophils purified by density-gradient centrifugation exhibited significant NET levels independent of the surfaces (Fig. 4A). This was anticipated, as the density-gradient purification method had previously been reported to induce neutrophils to undergo NETosis[26]. The immunomagnetic separation method showed no significant increase in NET levels on either surface, regardless of the donor's diabetic status (Fig. 4B).
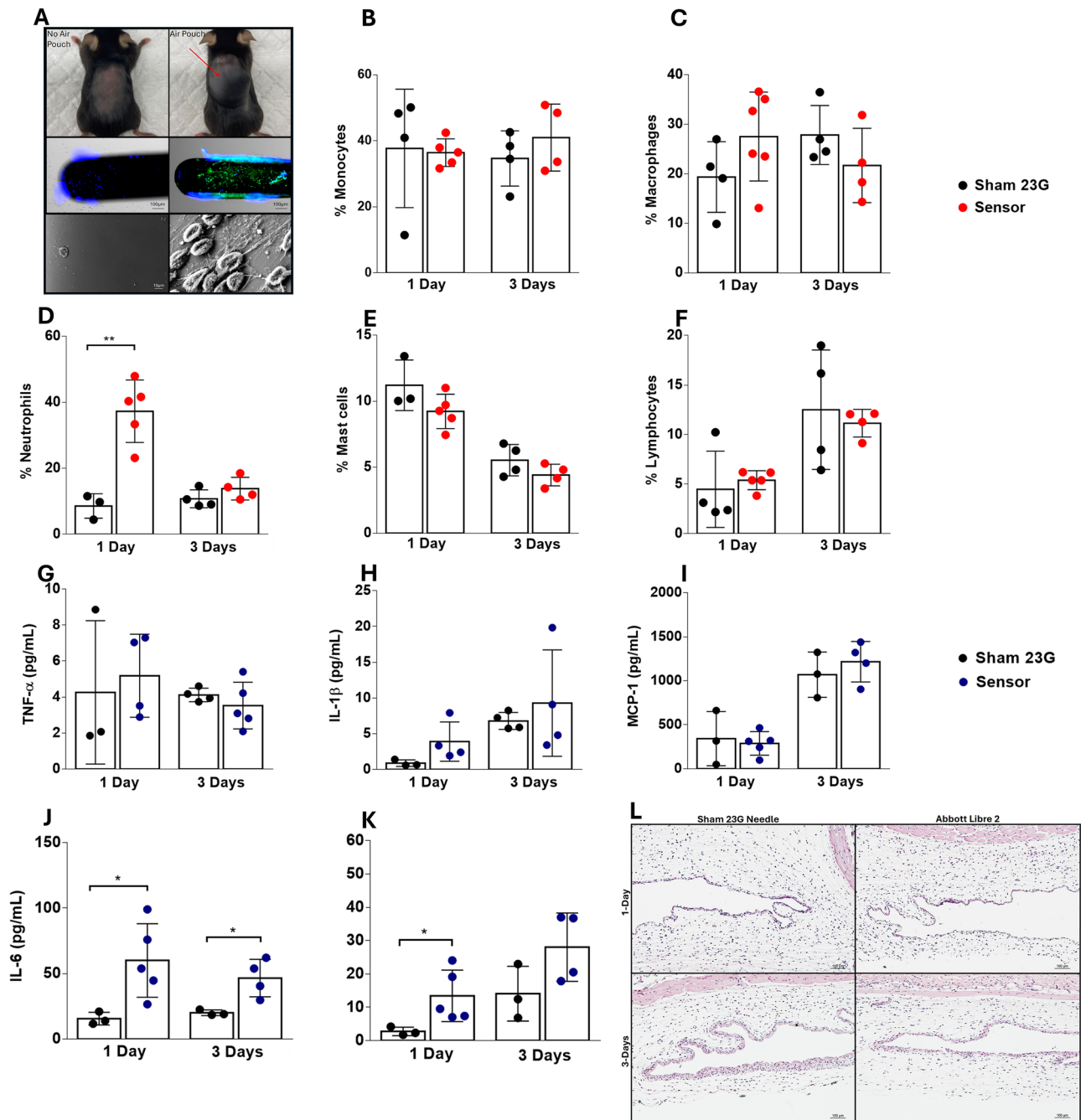
Fig. 2 | Detection of extracellular trap (ET) formation via immunohistochemistry in swine skin. ET was the predominant response in the sensor tissue on day 1 and was detectable for 7- and 14-days following sensor insertion. ET levels diminished with the dominance of fibrosis at 21 days after sensor insertion. DAPI staining represents DNA (1×) magnification, with the scale bar representing 1 mm. NETosis was visualized using the DNA stain DAPI (blue) and co-staining with the neutrophil-specific marker elastase (blue) and myeloperoxidase (MPO) (red) at day 1 with magnification (20×), scale bar indicating 100 μm. The stain elastase was replaced with citrullinated histone H3 (green) for weeks 1 to 3.

Discussion

The host's response to dermal penetration by a glucose sensor will affect a device's sensitivity, performance, and longevity. Anomalous sensor performance immediately following implantation is well-described and is attributed to erythrocytes consuming glucose adjacent to the sensor surface[27], the consumption of glucose by inflammatory cells[28], or local blood flow and tissue perfusion restriction due to "sleeping position"[29]. Our studies suggest that insertion trauma and subsequent NETosis are additional factors contributing to suboptimal sensor performance in the early hours following insertion (Fig. 2). Specifically, our data demonstrate that the tissue injury

caused by the insertion mechanism initiates an inflammatory response through NET formation, compromising the otherwise favorable biocompatible sensor coating. Sensor insertion into porcine skin initiates an immune reaction driven initially by a response to the foreign device and NET formation (Figs. 1 and 2). These observations suggest that NETosis has a strong influence on the subsequent host immune response secondary to the biomaterial in the early hours following sensor insertion. While NETosis is essential for pathogen clearance by releasing decondensed chromatin and granular contents to the extracellular space, excessive NET formation, observed following sensor insertion, can amplify tissue damage and limit

Fig. 3 | Sensor insertion in mice with and without an air pouch. A Representative images of mice featuring the presence or absence of an air pouch, along with related fluorescent and SEM images. **B–F** Percentages of immune cell populations in air pouch lavage fluid after glucose sensor implantation or sham injury (23 G needle puncture) at 1 and 3 days. **G–K** Cytokine levels in air pouch lavage fluid following glucose sensor or sham implantation (23 G needle poke) at 1- and 3-day time points. **L** Representative H&E images of the air pouch after glucose sensor or sham implantation (23 G needle poke) at 1 and 3 days. Data are presented as the mean ± SD of per group. Statistical comparison were performed using t-test with Welch's correction. $p < 0.05$ (*); $p < 0.005$ (**).
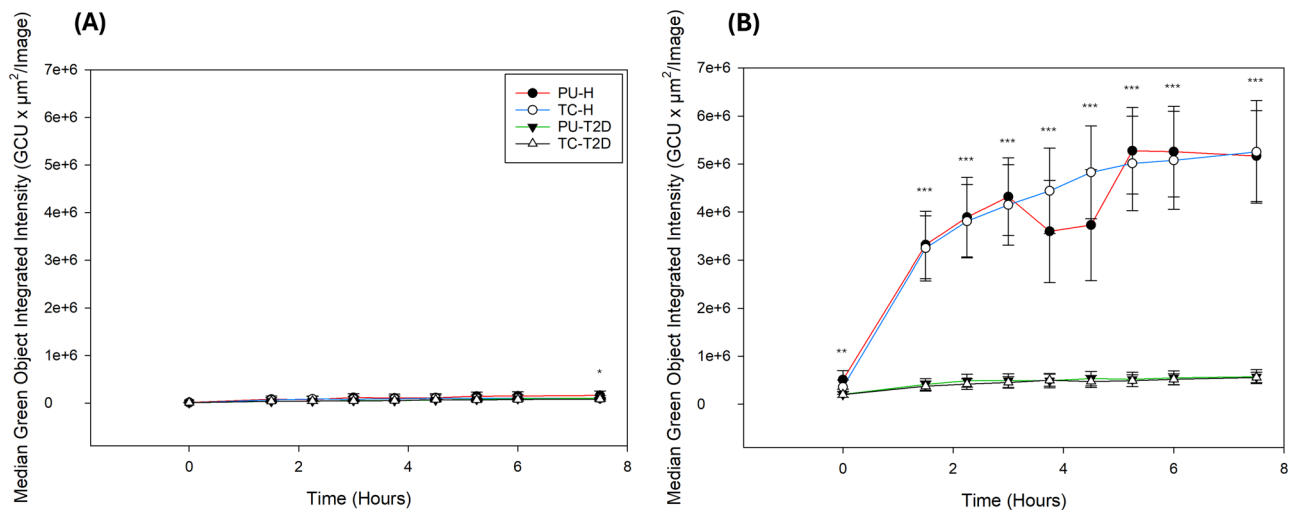
device functionality[18–22,25]. Thus, future studies should investigate the effect of reducing the impact of device insertion and its associated subsequent NETosis.

Quantification of blood vessel regression (Fig. 1B) uncovers a clear timeline linking glucose sensor implantation to vascular regression, resulting in a fibrotic microenvironment by Day 21 (Fig. 1A, B). Twenty-one days post-implantation, vessels are only observed around the periphery of the device, where fibroblast recruitment and collagen deposition occur, resulting in a dense, fibrous capsule forming around the implant (Fig. 1A). This vessel regression could impair the accuracy of CGM devices, as they measure interstitial blood glucose levels. Consequently, vessel regression might

hinder glucose transport between blood vessels and interstitial fluid, increasing the lag time between blood and interstitial glucose levels. This may cause delays and discrepancies in glucose readings over time. The encapsulation isolates the device from the body, forming a physical barrier and scar tissue that makes this tissue site unavailable for future diabetes management devices.

It is often believed that the biocompatibility of the implanted material influences the severity of the tissue response to device insertion[30,31]. The mouse air pouch model, well known for its use in biocompatibility studies, provides a controlled environment for examining the host's immune response to the implanted material, including leukocyte influx and cytokine

Fig. 4 | The tendency of isolated human neutrophils from healthy donors and individuals with type 2 diabetes to form extracellular traps. Cells were isolated using the EasySep Direct Human Neutrophil Isolation Kit (**A**) and Polymorphoprep gradient isolation (**B**). Signals were measured in green fluorescent units (GFU) multiplied by the surface area per image. Error bars indicate ± the standard deviation from the median. (***) Statistical differences were observed between healthy donors and individuals with type 2 diabetes, regardless of whether the tissue culture well was coated with polyurethane (PU) or tissue culture coating (TC). (**) Statistical differences were noted between healthy donors and individuals with type 2 diabetes when isolated using Polymorphoprep gradient isolation, specifically in coated wells. (*) Statistical differences were found between neutrophils from healthy donors (H) in coated wells and neutrophils from individuals with type 2 diabetes (T2D) in non-coated wells when isolated using the EasySep Direct Human Neutrophil Isolation Kit.

levels assessed via air pouch lavage[24]. Mice were used to evaluate the inflammatory response to the sensor material. Unlike clinical devices, sensors were manually inserted using a minimally invasive 23-gauge needle, avoiding applicator-induced trauma. This method was used for insertions with and without an air pouch (Fig. 3A). Only sensors placed in the air pouch showed NETosis by day 1, confirmed by SEM (Fig. 3A), suggesting that air pouch-induced trauma primes the material surface for NETosis.

Following mouse lavage analysis, neutrophils at 1-day post-insertion showed statistical significance in sensor-induced leukocyte influx in the murine air pouch (Fig. 3D). The primary inflammatory markers elevated after skin injury include IL-6 for both days investigated and KC/GRO for day one post-material insertion (Fig. 3J, K). These markers play a critical role in mediating the inflammatory response and subsequent wound-healing processes. All leukocyte subpopulations, apart from neutrophils, are insignificant compared to the sham group. The induction of a mouse air pouch triggers an acute inflammatory response. Studies have demonstrated that neutrophil activation and NETosis occur on a variety of biomaterial surfaces, and that these processes are observed even with coatings designed to minimize immune activation[17,32,33]. Thus, the insertion process itself is a critical determinant of the early immune response, challenging the notion that biocompatibility alone dictates the intensity and severity of tissue reactions to implanted devices[17,32–34].

Type 2 Diabetes (T2D) impacts NET formation due to the chronic hyperglycemic environment and associated metabolic imbalances. Several studies have demonstrated that diabetes enhances NETosis through hyperglycemia-induced metabolic changes and the generation of reactive oxygen species via NADPH oxidase, which is necessary for NETosis[35,36]. It is now known that constitutive activation of neutrophils leads to abundant NETs in T2D subject plasma. However, our analyses showed that neutrophils derived from the blood of T2D diabetes populations did not initiate NETosis on the tested polyurethane surface, irrespective of the isolation method (Fig. 4). Although these data contradicted our initial hypothesis, the lack of NETosis in vitro on the tested surfaces may be attributable to the metabolic and functional alterations in T2D neutrophils resulting from the hyperglycemic and pro-inflammatory environment characteristic of diabetes[37,38]. Hyperglycemia leads to metabolic reprogramming in neutrophils, which affects their ability to form effective NETs. Farhan et al. reported that hyperglycemia-mediated ROS production primes neutrophils

for NETosis; however, this process is dysregulated, leading to impaired phagocytosis and reduced pathogen killing[35,38]. This implies that while NET formation is increased, the functional quality and regulatory response of these NETs are impaired. Although NETs are constitutively expressed in T2D, they are less effective in pathogen clearance, thus contributing to the increased susceptibility to infections and delayed wound healing[39]. Carestia et al. observed normalization of NET functionality following metabolic control and hypothesized that the increased NETosis is not the consequence of impaired glycemic control but is more likely due to a pro-inflammatory environment[40]. For our T2D donor population, we did not differentiate between controlled and poorly controlled diabetes, which are defined as a glycated hemoglobin (HbA1c) level of 7.0% or lower and greater than 9.0%, respectively[41]. Thus, future studies should enroll a T2D patient population, considering HbA1c levels. This knowledge could facilitate the development of strategies and surface modifications to enhance neutrophil response in patients with diabetes, while addressing impaired NETosis. Another study limitation is that we did not include T1D patients. Studies recruiting T1D subjects have reported that NET formation is altered, but not necessarily increased[42,43]. Accounting for variations based on age, race, and other factors, T1D populations generally have similar HbA1c levels to T2D populations[41,44–46].

Our findings highlight the crucial role of the host immune response, particularly NETosis, in influencing the potential function and longevity of transdermal glucose sensors. The insertion process itself, rather than just the material used, primarily triggers acute inflammation, tissue damage, and NET formation, all of which could impair early sensor performance. Data from our study suggest that insertion-induced NETosis initiates a chain of immune responses that ultimately lead to vascular regression and fibrotic encapsulation, as evidenced by vascular remodeling and collagen deposition over 21 days. In addition, while chronic hyperglycemia in T2D patients is known to prime neutrophils for NETosis, our in vitro tests show that neutrophils from T2D patients do not initiate NETosis on polyurethane surfaces. This indicates a disconnect between systemic NET levels and biomaterial-specific neutrophil responses, likely due to metabolic reprogramming and immune imbalance in diabetes. These results underscore the importance of understanding how metabolic status influences the innate immune response at the device-tissue interface. Overall, our findings support the development of improved sensor insertion techniques and surface

modifications that reduce the acute inflammatory response, especially NETosis, thereby maintaining sensor function, reducing fibrotic encapsulation, and ultimately preserving healthy tissue to extend device lifespan. Future research should categorize diabetic patients based on glycemic control and diabetes type to better tailor biomaterial design and therapies, thereby improving device integration and outcomes.

Methodology

Swine studies. Six Healthy Yucatan pathogen-free mini pigs, three males, and females weighing 50 kg to 89 kg, were investigated (Premier Bioresources/S&S Farms, Indiana). These animals were housed in multiple pens, separated by sex, during the 7-day acclimation period at 22–25 °C with a relative humidity of 30–70%. Swine were fed twice daily with LabDiet Mini-Pig High Fortification Grower 5L80 (Frontier Distributing, MI, US) diet with free access to tap water. A 12-h fast preceded the insertion of the commercial Freestyle Libre 2 glucose sensors (ADW Diabetes, Pompano Beach, FL, US). On the sensor insertion date, the pigs were anesthetized with an intramuscular combination of Midazolam (0.4 mg/kg, Hospira Inc., Lake Forest, IL), Xylazine (1.0 mg/kg), and Butorphanol (0.2 mg/kg, Zoetis, Parsippany, NJ, US). Additional maintenance anesthesia with an isoflurane/oxygen mixture was supplemented. The umbilical region was shaved and sponged-washed with warm water. The area was coated with Skin Tac (Torbot Group Inc., Warwick, RI, US) to increase sensor adhesion and allowed to dry. Up to twelve Libre 2 were inserted subcutaneously into the lower abdominal region and secured with Elastikon tape (Johnson and Johnson, New Brunswick, NJ) followed by a sheet of Tegaderm Transparent Film Dressing (3 M, Maplewood, MN, US). Animals were given the reversal agent anti-sedan (Zoetis, Parsippany, NJ) and single-housed. Sensors were implanted subcutaneously for 1-, 7-, 14-, or 21 days. Sensor tissue was obtained through an 8-mm SHARD premium+ Disposable Biopsy Punch (AD Surgical, CA, US), and wounds were closed with a single cruciate pattern suture. Biopsies were processed for histological analysis. All studies were conducted with approval from the Institutional Animal Care and Use Committee at Wayne State University. We have complied with all relevant ethical regulations for animal use.

Histological evaluations. Following the biopsy, the tissue was placed in Zinc Fixative (BD Pharmingen, San Diego, CA) for 24 h, followed by standard embedding and tissue sectioning preparation. Tissue samples were stained with a standard Hematoxylin and Eosin (H&E) (Fisher Scientific, Waltham, MA) and Masson's trichrome stain (Epredia, MI, US). Neovascularization was analyzed by staining endothelial cells with anti-CD31 (Abcam, Cambridge, UK, ab28364). Fluorescent antibody immunohistochemistry staining was employed to evaluate Neutrophil extracellular DNA traps. It included a DAPI stain (Electron Microscopy Sciences Fluoro-Gel II, Hatfield, PA), Histone 3 (H3), or Elastase stain (Abcam, Cambridge, UK, ab3594 & ab68672, respectively). This was followed with secondary antibody staining of 5/6-fluorescein isothiocyanate (FITC) (ABcam, Cambridge, UK, ab7086). Myeloperoxidase (MPO) staining (R&D Systems Inc., Minneapolis, MN, AF3667) included secondary staining with Anti-goat IgG-NL637 (R&D Systems Inc., Minneapolis, MN, NL002). Imaging and analysis were performed on a Nikon Eclipse Ni microscope and NIS Elements Imaging software.

Quantification of blood vessel regression

The extent of blood vessel regression was assessed using ImageJ. After calibrating the image scale to 100 μm, linear measurements were taken from each blood vessel to the glucose sensor–tissue interface. Six blood vessels were selected per image—three from each lateral side—across different regions to ensure spatial representation.

Mice, air pouch generation, and glucose sensor insertion. C57BL/6 mice, at least fifteen females and fifteen males, 8–12 weeks of age (Jackson Laboratory, Bar Harbor, ME, US), were maintained under temperature and light-controlled conditions (20–24 °C, 12 h light-dark cycle), receiving food and water ad libitum. Following an acclimation period, the animal's dorsal surface was shaved, and an air pouch was created using a subcutaneous injection of 3 mL of sterile, filtered air[47,48]. Animals were stratified by weight and then randomly assigned to each time point group. A 23-gauge needle pierced the caudal surface of the air pouch, and the sensing element without its applicator and circuit board was gently inserted. A 23-gauge needle poke was used as a sham control. Animals undergoing glucose sensor implants without the air pouch received 100 μL sterile saline at the sensor insertion site[49–51]. Mice were sacrificed at 1-day and 3-days post-sensor insertion to withdraw the sensor and to lavage the air pouch. The lavage fluid was stored in a −70 °C freezer for subsequent cytokine evaluation.

Primary human neutrophils isolation

Peripheral blood was collected via venipuncture from healthy adult volunteers and individuals with type 2 diabetes (T2D) using K2EDTA VACUETTE 4 mL collection tubes (Greiner Bio-One, Monroe, NC). This study involved four T2D donors who had a confirmed history of T2D and had been non-smokers for at least one year (age range 50 to 72 years). In addition, four healthy subjects with no history of smoking and diabetes were included. The Wayne State University Institutional Review Board approved this study, and written informed consent was obtained from all participants. All ethical regulations relevant to human research participants were followed.

Neutrophils were isolated using the EasySep Direct Human Neutrophil Isolation Kit (StemCell Technologies, Cambridge, MA). The purified neutrophils were collected and placed into fresh Roswell Park Memorial Institute 1640 medium with GlutaMAX™ supplement (Gibco-Thermo Fisher Scientific, Waltham, MA). Using the Polymorphprep (Serumwerk Bernburg, Germany), anticoagulated whole blood was gently layered over equal volumes of Polymorphprep and centrifuged at $500 \times g$ for 30 min at 20 °C. Subsequently, neutrophils were transferred to a 0.45% NaCl solution to restore osmolality. Red blood cells remaining in the sample were lysed with ACK Lysing Buffer (Gibco-Thermo Fisher Scientific, Waltham, MA). Isolated human neutrophils were resuspended in Roswell Park Memorial Institute 1640 medium plus L-Glutamine without phenol red (Gibco-Thermo Fisher Scientific, Waltham, MA).

Sensor cell surface attachment in vitro

Neutrophils (1.0×10^6 cells) isolated using the EasySep method were placed in Roswell Park Memorial Institute 1640 medium supplemented with GlutaMAX™ (Gibco-Thermo Fisher Scientific, Waltham, MA). The cells were incubated with the sensing element of the continuous blood glucose monitor for 45 minutes. This was followed by two washes with Dulbecco's phosphate-buffered saline (DPBS) (Gibco-Thermo Fisher Scientific, Waltham, MA), after which they were submerged in Dulbecco's modified Eagle medium (DMEM) (Gibco-Thermo Fisher Scientific, Waltham, MA) containing Hoechst 33342 trihydrochloride trihydrate and Cytotox Green live and dead cell stain for 15 min. Next, sensors were added to a well containing only Cytotox Green and cell media for three subsequent imaging time points at 3, 6, and 24 h, using a BZ-X810 fluorescence microscope (Keyence, Itasca, IL).

Polyurethane surface preparation

Polyurethane-coated tissue culture plates were utilized to replicate the sensor surfaces. Thermoplastic polyurethane (TPU) resin (Lubrizol, Wickliffe, OH) pellets were added to tetrahydrofuran (Fisher Scientific, Waltham, MA) at a concentration of 7% w/w and fully dissolved at 40 °C. After dissolution, 150 μL of liquefied resin was pipetted into 12 wells of black glass-bottom 24-well culture plates (Fisher Scientific, Waltham, MA) and allowed to cure at 50 °C for 72 h. Following curing, each plate was washed three times with sterile Dulbecco's Phosphate Buffered Saline and UV sterilized for 35 min. Plates were stored in a desiccator until use.

Article

Live neutrophil cell imaging

Human neutrophils (2×10^5 cells) suspended in media with 250 nM of Cytotox green (Sartorius, Goettingen, Germany) were added to a black glass-bottom 24-well plate, including the TPU-coated plate. For 10 h, the plates were imaged every 45 min (20x) using the Sartorius Incucyte SX5, and the data was analyzed using the Sartorius Incucyte SX5 image analysis software.

Scanning electron microscopy assessing material cell-surface

Scanning electron microscopy (SEM) was used to examine cell attachment and ET formation of the sensor implanted in mice. Upon retrieval, the sensors were fixed for 2 h in a solution of 2% glutaraldehyde and 2% paraformaldehyde in 0.1 M cacodylate buffer, followed by two washes in double-distilled water. The sensors then underwent secondary fixation by soaking in a 2% osmium tetroxide solution for 1 h, followed by additional washes with double-distilled water before being placed in ethanol for dehydration. Samples were prepared using a Quorum K850 critical point dryer and mounted on carbon tape. Sputter coating with gold-palladium was performed using a Safematic CCu-010 high-vacuum compact coating unit. Surface imaging was conducted with a Zeiss GeminiSEM 300 SE2 detector. Scanning electron microscopy sample processing and imaging were carried out at the Wayne State University Microscopy, Imaging, and Cytometry Resource Core.

Cytokine analysis for mouse lavage fluids

Mouse lavage fluids were collected after 1 and 3 days of Libre 2 sensor insertion into the air pouch and compared to the sham group. The custom mouse V-Plex assay was designed for a multiplex panel of cytokines and chemokines, including IL-1β, IL-6, KC/GRO, TNF-α, IL-10, IFN-γ, and MCP-1. The levels of each analyte were measured using the electrochemiluminescent detection method following the manufacturer's instructions (MesoScale Discovery, MSD).

Leukocyte fluorescence-activated cell sorting (FACS) analysis

Following 1 and 3 days, leukocytes within the air pouch model were identified as previously described[24]. Flow cytometry analysis was performed by the microscopy, imaging, and cytometry core laboratory on a BD LSR II at Wayne State University. The gating strategy can be found in supplementary materials (Supplementary Fig. 3).

Statistics and reproducibility

Statistical analysis was conducted using SigmaPlot version 15. P-values below 0.05 were considered significant. Data normality was assessed with the Shapiro-Wilk normality test. The Student's T-test was applied to all normally distributed data, while the Mann-Whitney Rank Sum Test was utilized for all non-normally distributed data. When comparing different time points, a one-way ANOVA was performed with a post hoc Holm-Sidak pairwise multiple comparison to determine group differences.

Reporting summary

Further information on research design is available in the Nature Portfolio Reporting Summary linked to this article.

Data availability

The authors declare that all data supporting the findings of the study are available within the paper and Supplementary Data 1 information files.

References

1. David, P., Singh, S. & Ankar, R. A comprehensive overview of skin complications in diabetes and their prevention. *Cureus* **15**, e38961 (2023).
2. Lu, Y. et al. Vascular complications of diabetes: a narrative review. *Medicine* **102**, e35285 (2023).
3. Bergenstal, R. M. et al. Evolution of the artificial pancreas: components and integration-CGMs, insulin, and AP systems. *J. Diabetes Sci. Technol.* **19**, 883–894 (2025).
4. Calhoun, P., Price, D. & Beck, R. W. Glycemic improvement using continuous glucose monitoring by baseline time in range: subgroup analyses from the DIAMOND type 1 diabetes study. *Diabetes Technol. Ther.* **23**, 230–233 (2021).
5. Maiorino, M. I. et al. Effects of continuous glucose monitoring on metrics of glycemic control in diabetes: a systematic review with meta-analysis of randomized controlled trials. *Diabetes Care* **43**, 1146–1156 (2020).
6. American Diabetes Association Professional Practice, C. 13. Older adults: standards of care in diabetes—2024. *Diabetes Care* **47**, S244–S257 (2024).
7. Klueh, U. Analysis: on the path to overcoming glucose-sensor-induced foreign body reactions. *J. Diabetes Sci. Technol.* **7**, 452–454 (2013).
8. Klueh, U., Kaur, M., Montrose, D. C. & Kreutzer, D. L. Inflammation and glucose sensors: use of dexamethasone to extend glucose sensor function and life span in vivo. *J. Diabetes Sci. Technol.* **1**, 496–504 (2007).
9. Koh, A., Nichols, S. P. & Schoenfisch, M. H. Glucose sensor membranes for mitigating the foreign body response. *J. Diabetes Sci. Technol.* **5**, 1052–1059 (2011).
10. Klueh, U. et al. Impact of CCL2 and CCR2 chemokine/receptor deficiencies on macrophage recruitment and continuous glucose monitoring in vivo. *Biosens. Bioelectron.* **86**, 262–269 (2016).
11. Klueh, U., Qiao, Y., Frailey, J. T. & Kreutzer, D. L. Impact of macrophage deficiency and depletion on continuous glucose monitoring in vivo. *Biomaterials* **35**, 1789–1796 (2014).
12. Novak, M. T., Yuan, F. & Reichert, W. M. Macrophage embedded fibrin gels: an in vitro platform for assessing inflammation effects on implantable glucose sensors. *Biomaterials* **35**, 9563–9572 (2014).
13. Rosenberg, L. K. et al. A comparison of human and porcine skin in laser-assisted drug delivery of chemotherapeutics. *Lasers Surg. Med* **53**, 162–170 (2021).
14. Summerfield, A., Meurens, F. & Ricklin, M. E. The immunology of the porcine skin and its value as a model for human skin. *Mol. Immunol.* **66**, 14–21 (2015).
15. Anderson, J. M., Rodriguez, A. & Chang, D. T. Foreign body reaction to biomaterials. *Semin Immunol.* **20**, 86–100 (2008).
16. Pertiwi, K. R. et al. Extracellular traps derived from macrophages, mast cells, eosinophils and neutrophils are generated in a time-dependent manner during atherothrombosis. *J. Pathol.* **247**, 505–512 (2019).
17. Fetz, A. E. & Bowlin, G. L. Neutrophil extracellular traps: inflammation and biomaterial preconditioning for tissue engineering. *Tissue Eng. Part B Rev.* **28**, 437–450 (2022).
18. Herre, M., Cedervall, J., Mackman, N. & Olsson, A. K. Neutrophil extracellular traps in the pathology of cancer and other inflammatory diseases. *Physiol. Rev.* **103**, 277–312 (2023).
19. Hidalgo, A. et al. Neutrophil extracellular traps: from physiology to pathology. *Cardiovasc Res.* **118**, 2737–2753 (2022).
20. Manoj, H. et al. Cytokine signalling in formation of neutrophil extracellular traps: implications for health and diseases. *Cytokine Growth Factor Rev.* https://doi.org/10.1016/j.cytogfr.2024.12.001 (2024).
21. Poli, V. & Zanoni, I. Neutrophil intrinsic and extrinsic regulation of NETosis in health and disease. *Trends Microbiol.* **31**, 280–293 (2023).
22. Gu, W. et al. The role of extracellular traps released by neutrophils, eosinophils, and macrophages in asthma. *Respir. Res.* **25**, 290 (2024).
23. Kesserwan, S. et al. Inflammation at site of insulin infusion diminishes glycemic control. *J. Pharm. Sci.* **111**, 1952–1961 (2022).

24. Kesserwan, S. et al. Advancing continuous subcutaneous insulin infusion in vivo: new insights into tissue challenges. *J. Biomed. Mater. Res. A* **109**, 1065–1079 (2021).

25. Fadini, G. P. et al. NETosis delays diabetic wound healing in mice and humans. *Diabetes* **65**, 1061–1071 (2016).

26. Blanter, M. et al. Method matters: effect of purification technology on neutrophil phenotype and function. *Front. Immunol.* **13**, 820058 (2022).

27. Klueh, U. et al. Metabolic biofouling of glucose sensors in vivo: role of tissue microhemorrhages. *J. Diabetes Sci. Technol.* **5**, 583–595 (2011).

28. Novak, M. T., Yuan, F. & Reichert, W. M. Predicting glucose sensor behavior in blood using transport modeling: relative impacts of protein biofouling and cellular metabolic effects. *J. Diabetes Sci. Technol.* **7**, 1547–1560 (2013).

29. Mensh, B. D., Wisniewski, N. A., Neil, B. M. & Burnett, D. R. Susceptibility of interstitial continuous glucose monitor performance to sleeping position. *J. Diabetes Sci. Technol.* **7**, 863–870 (2013).

30. Avery, D. et al. Immune cell response to orthopedic and craniofacial biomaterials depends on biomaterial composition. *Acta Biomater.* **161**, 285–297 (2023).

31. Cerqueira, A. et al. Evaluation of the inflammatory responses to sol-gel coatings with distinct biocompatibility levels. *J. Biomed. Mater. Res. A* **109**, 1539–1548 (2021).

32. Abaricia, J. O., Shah, A. H., Musselman, R. M. & Olivares-Navarrete, R. Hydrophilic titanium surfaces reduce neutrophil inflammatory response and NETosis. *Biomater. Sci.* **8**, 2289–2299 (2020).

33. Jhunjhunwala, S. et al. Neutrophil Responses to Sterile Implant Materials. *PLoS ONE* **10**, e0137550 (2015).

34. Gomes, Y. V. R. et al. Biological responses to biomaterials: a review. *Braz. J. Med. Biol. Res.* **58**, e14599 (2025).

35. Farhan, A. et al. Spontaneous NETosis in diabetes: A role of hyperglycemia mediated ROS and autophagy. *Front. Med.* **10**, 1076690 (2023).

36. Joshi, M. B. et al. Elevated homocysteine levels in type 2 diabetes induce constitutive neutrophil extracellular traps. *Sci. Rep.* **6**, 36362 (2016).

37. Jin, L. et al. Neutrophil extracellular traps (NETs)-mediated killing of carbapenem-resistant hypervirulent Klebsiella pneumoniae (CR-hvKP) are impaired in patients with diabetes mellitus. *Virulence* **11**, 1122–1130 (2020).

38. Joshi, M. B. et al. Glucose induces metabolic reprogramming in neutrophils during type 2 diabetes to form constitutive extracellular traps and decreased responsiveness to lipopolysaccharides. *Biochim. Biophys. Acta Mol. Basis Dis.* **1866**, 165940 (2020).

39. Yang, S. et al. Neutrophil extracellular traps delay diabetic wound healing by inducing endothelial-to-mesenchymal transition via the Hippo pathway. *Int. J. Biol. Sci.* **19**, 347–361 (2023).

40. Carestia, A. et al. NETosis before and after hyperglycemic control in type 2 diabetes mellitus patients. *PLoS ONE* **11**, e0168647 (2016).

41. Soongsathitanon, J., Umsa-Ard, W. & Thongboonkerd, V. Proteomic analysis of peripheral blood polymorphonuclear cells (PBMCs) reveals alteration of neutrophil extracellular trap (NET) components in uncontrolled diabetes. *Mol. Cell Biochem.* **461**, 1–14 (2019).

42. Aukrust, S. G. et al. NETosis in long-term type 1 diabetes mellitus and its link to coronary artery disease. *Front. Immunol.* **12**, 799539 (2021).

43. Bissenova, S. et al. NET proteome in established type 1 diabetes is enriched in metabolic proteins. *Cells* https://doi.org/10.3390/cells12091319 (2023).

44. American Diabetes Association Professional Practice, C. 1. Improving care and promoting health in populations: standards of care in diabetes—2025. *Diabetes Care* **48**, S14–S26 (2025).

45. American Diabetes Association Professional Practice, C. 3. Prevention or delay of diabetes and associated comorbidities: standards of care in diabetes—2025. *Diabetes Care* **48**, S50–S58 (2025).

46. Salam, M. et al. A comparison of continuous glucose monitoring estimated hemoglobin A1c in adults with type 1 or type 2 diabetes. *Diabetes Technol. Ther.* **25**, 178–185 (2023).

47. Kesserwan, S., Mao, L., Sharafieh, R., Kreutzer, D. L. & Klueh, U. A pharmacological approach assessing the role of mast cells in insulin infusion site inflammation. *Drug Deliv. Transl. Res.* **12**, 1711–1718 (2022).

48. Kesserwan, S., Sadagurski, M., Mao, L. & Klueh, U. Mast cell deficiency in mice attenuates insulin phenolic preservative-induced inflammation. *Biomedicines* **11**, 2258 (2023).

49. Klueh, U., Dorsky, D. I. & Kreutzer, D. L. Uses of vascular endothelial cell growth factor gene transfer to enhance biosensor function in vivo. *J. Biomed. Mater. Res.* **67A**, 1072–1086 (2003).

50. Klueh, U., Dorsky, D. I. & Kreutzer, D. L. Enhancement of implantable glucose sensor function in vivo using gene transfer-induced neovascularization. *Biomaterials* **26**, 1155–1163 (2005).

51. Klueh, U. et al. Continuous glucose monitoring in normal mice and mice with prediabetes and diabetes. *Diabetes Technol. Ther.* **8**, 402–412 (2006).

Author contributions

K.A.W.: Investigation, methodology, study execution, data analysis, figure creation, writing, and editing. P.S.C.: Methodology, cell isolation, data analysis, writing, and editing. J.G.D.: Study execution, flow cytometry analysis, and figure creation. J.C.: Figure creation. T.K.: Figure creation and editing. D.K.: Conceptualization and methodology. U.M.: Conceptualization, methodology, investigation, writing, editing, funding acquisition, and supervision.

Competing interests

The authors declare no competing interests.

Additional information

Supplementary information The online version contains supplementary material available at https://doi.org/10.1038/s42003-025-09062-z.

Correspondence and requests for materials should be addressed to Ulrike Klueh.

Peer review information *Communications Biology* thanks Rachel Beatty and Hongyan Xie for their contribution to the peer review of this work. Primary Handling Editors: Dr Ophelia Bu and Dr Dario Ummarino.

Reprints and permissions information is available at http://www.nature.com/reprints

Publisher's note Springer Nature remains neutral with regard to jurisdictional claims in published maps and institutional affiliations.